nature geoscience

SUPPLEMENTARY INFORMATION

DOI: 10.1038/NGEO2546

Spectral evidence for hydrated salts in recurring slope lineae on Mars

Authors: Lujendra Ojha[1*], Mary Beth Wilhelm[1, 2], Scott L. Murchie[3], Alfred S. McEwen[4], James J. Wray[1], Jennifer Hanley[5], Marion Massé[6], Matt Chojnacki[4],

Affiliations:
1School of Earth and Atmospheric Sciences, Georgia Institute of Technology, Atlanta, Georgia, USA.
2Space Science and Astrobiology Division, NASA Ames Research Center, Moffett Field, California, USA.
3Applied Physics Laboratory, Laurel, Maryland, USA.
4Lunar and Planetary Laboratory, University of Arizona, Tucson, Arizona, USA.
5Department of Space Studies, Southwest Research Institute, Boulder, Colorado, USA.
6Laboratoire de Planétologie et Géodynamique, Nantes, France.

This SOM contains (1) a general description of our dataset and methodology, (2) details of our atmospheric correction, validation approach and spectral mixture model, (3) supplementary figures to illustrate RSL activity and areas analyzed in CRISM images, and (4) Tables S1 and S2 that list the data used in this work.

(1) Dataset and Methodology: CRISM[1] full-resolution targeted (FRT ~18 m/pix), full-resolution short (FRS ~18 m/pix), and Along Track Oversampled (ATO 18 m/pix, with enhanced overlap to support processing to ~6 m/pixel) observations at Infrared (IR: 1.0-3.9 μm) wavelengths coordinated with HiRISE observations were used to examine the spectral characteristics of RSL. We chose not to inspect images in the VNIR detector range (0.4-1.0 μm), because our focus was clear evidence for or against signs of hydration, which is primarily detected using absorptions in the IR detector wavelength range. The CRISM images which were analyzed to study spectral characteristics of RSL described here are listed in Table S1, along with the coordinated HiRISE images in which the lineae were initially identified. Table S1 also lists the central latitude and longitude of the images along with their solar longitude (L_s), and exact coordinates for the location of spectra presented here. Table S2 lists exact coordinates of the denominator areas used to create the ratio spectra of RSL shown here. CRISM I/F images were downloaded from PDS and were preprocessed using ENVI's (Exelis Visual

Information Solutions) CRISM Analysis Tool (CAT)[2] to reduce atmospheric effects, and when necessary map project the images.

(2) Atmospheric Correction, Validation Approach, and Spectral Mixture Modeling:

A significant challenge in conducting a spectroscopic study of RSL is uncertainty in the precise location of the feature seen in HiRISE data within CRISM images. Most individual lineae are a few meters wide and several times narrower than a CRISM pixel, but for sites discussed here, individual lineae overlap so that their footprints occupy a footprint close to that of a CRISM pixel. Previous work inspected only averages of many CRISM pixels, such that absorptions present over smaller areas would have been significantly weakened due to areal mixing. Given uncertainty in the location of RSL in CRISM observations, we instead searched for evidence of hydration in areas of CRISM images where RSL are detected in higher-resolution coordinated HiRISE images. We used multiple volcano-scan[2] observations to divide out atmospheric gas absorptions. We then normalized the entire image by generating a mean spectrum from a spectrally neutral area in the CRISM image, and dividing the entire atmospherically-corrected image by that neutral area. Denominator areas typically consisted of a few hundred pixels. Additionally, we tested multiple denominator areas to confirm that any apparent absorption features were independent of that choice. Once a satisfactory ratio image was created, we inspected the approximate RSL area pixel-by-pixel to seek any signs of hydration. We observed areas with weak signs of hydration on and near RSL. Once these areas of enhanced hydration were identified, we normalized the spectra from a region of interest using a denominator area from the same detector column in the atmospherically corrected image (Table S2). Reduction in systematic noise was significant, and the depth of hydration absorption bands relative to noise increased.

We also designed a band-detection algorithm to objectively discriminate between signal and noise. We apply a smoothing (moving-average) filter to a normalized reflectance spectrum and remove

the continuum by dividing the original spectrum by a 7th order polynomial-fit continuum curve. A band-detection algorithm[3] was implemented with a threshold distance of at least 0.2 μm between subsequent bands. The width and depth of each band was calculated to find the approximate area within the band. Any band detected by the algorithm that has an area higher than the mean of all the "bands" at any wavelength was characterized as a real signature. In the particular case of Palikir crater, where a probable 2.15 μm absorption band is observed, the program identified the 1.9 μm absorptions as real for all 6 pixels (Fig. S2). In three cases out of the six, the program also identified the 2.15 μm absorption feature as a true signal. The flowchart for the algorithm is presented in Fig. S10.

Although the detection of 1.9-μm hydration bands in all areas presented is robust, we wanted to ensure that the observed absorption is time-variable and corresponds with RSL activity. In Palikir crater, four coordinated HiRISE/CRISM observations exist (Table S1). Spectral absorptions indicative of hydrated salts only occur in the images acquired towards the end of the southern summer, when fading RSL were observed to be longest and widest. At all other sites reported here, no other images from different seasons or Mars year exist to conduct a temporal study. Although we do not report negative results here, we conducted a spectroscopic search for signs of hydration in many other RSL sites (some with adequate temporal coverage), but no enhanced hydration absorptions were observed.

Spectral mixture models were created using laboratory spectra of various salts and reference spectra from each CRISM scene. In order to introduce similar noise content in our spectral mixture model as observed in spectra of RSL, we extracted reference spectra from areas listed in Table S2. These areas are in the same column as where we observed RSL hydration features, and were ratioed using the same denominator used for RSL spectra (hereafter referred to as "Martian soil" spectrum). A linear combination of Martian soil and various laboratory spectra of perchlorate, chlorate and chloride salts[4,5] was used to find the best matching spectra. In addition, we also ran a least-square regression

analysis between the observed spectrum and mixtures of various oxychlorine perchlorate species to match the position of the 1.4 μm absorption. The best match from the linear regression routine is shown in Fig. S5. While perchlorates can explain the narrowness of the observed absorptions, the inability to match the exact wavelength of the 1.48 μm band suggests the presence of an additional salt. We ran a similar least-square regression analysis between the observed spectrum and mixture of various sulfates to explore if there is a better match (Fig. S6). While the best fit linear-mixture of alunite (11.5%), jarosite (26.78%), Fe^{3+}-sulfate (19%) and Martian soil (42.65%) has an absorption band at ~1.48 μm, the linear mixture does not have an absorption band at 1.90 μm and 2.14 μm (Fig. S6).

References:

1. Murchie S. *et al.* Compact reconnaissance imaging spectrometer for Mars (CRISM) on Mars reconnaissance orbiter (MRO). *JGR: Planets* **112**, 1-57 (2007).

2. McGuire P.C. *et al*. An improvement to the volcano-scan algorithm for atmospheric correction of CRISM and OMEGA spectral data. *Planetary and Space Science* **57**, 809-815 (2009).

3. MATLAB and Statistics Toolbox Release 2012b, The MathWorks, Inc., Natick, Massachusetts, United States.

4. Hanley, J., V. F. Chevrier, R. S. Barrows, C. Swaffer, and T. S. Altheide. Near- and mid-infrared reflectance spectra of hydrated oxychlorine salts with implications for Mars, *JGR:Planets*, **120** (2015).

5. Crowley, J.K. Visible and near-infrared (0.4-2.5 μm) reflectance spectra of Playa evaporite minerals. *JGR* **96(B10)**, 16231-16240 (1991).

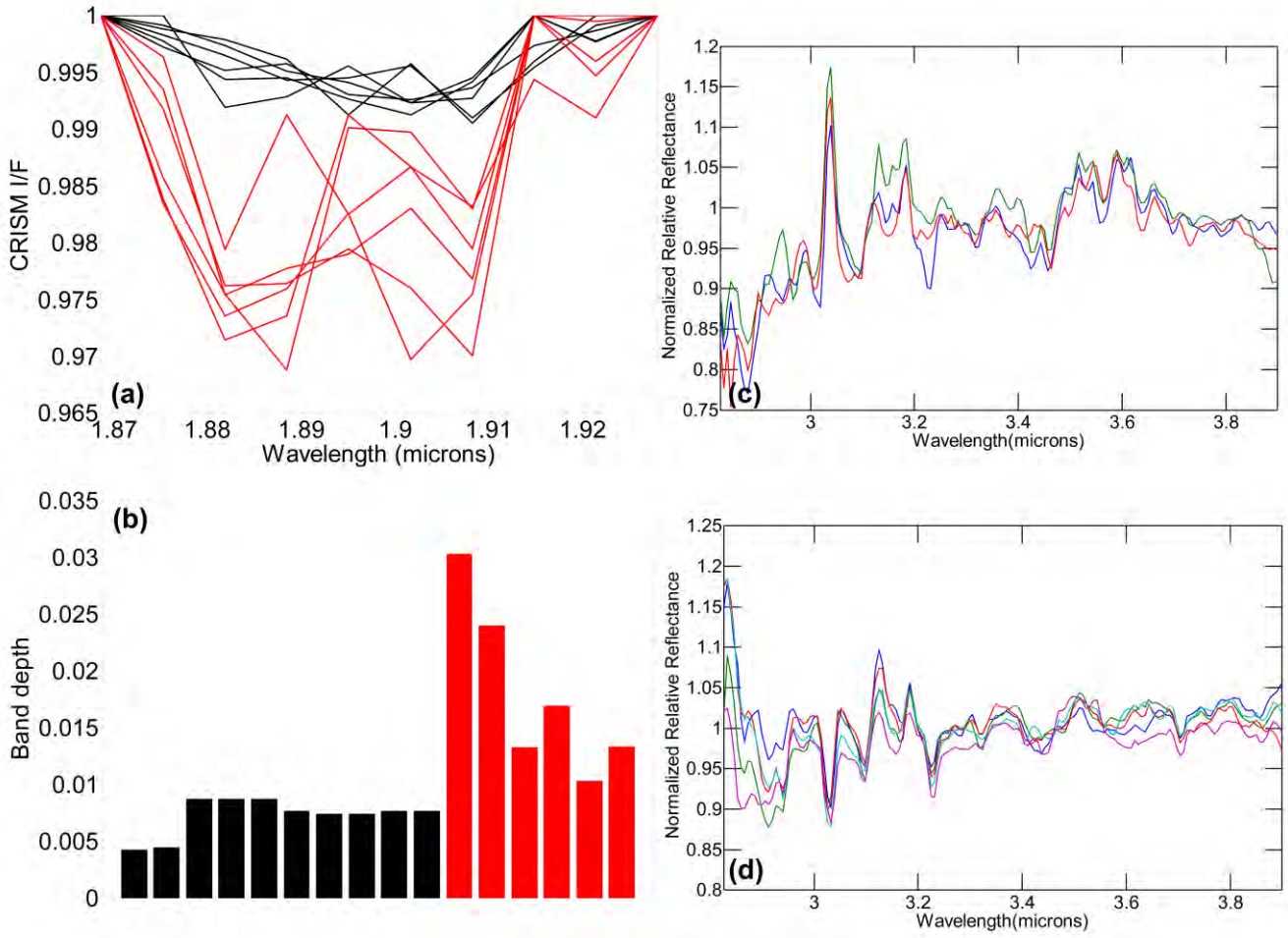

Fig S1. Spectra of RSL and a non-RSL region with similar albedo from CRISM FRT0002038F. **(a)** Continuum removed CRISM I/F reflectance spectra of the RSL pixels in red and non-RSL pixels in black showing absorption band at 1.9 µm. **(b)** Band-depth computed from the plot in (a). Red and Black corresponds to RSL and non-RSL slopes. **(c)** CRISM reflectance spectra ratioed to nearby non-RSL areas and normalized to relative reflectance at 2.6 µm. All RSL pixels show an enhanced absorption band at ~3 µm. **(d)** Same as (c) but for non-RSL regions with similar albedo. The latter spectra lack enhanced absorption bands at 1.4 µm, 1.9 µm and 3.0 µm (see Table S2 for the location of the spectra).

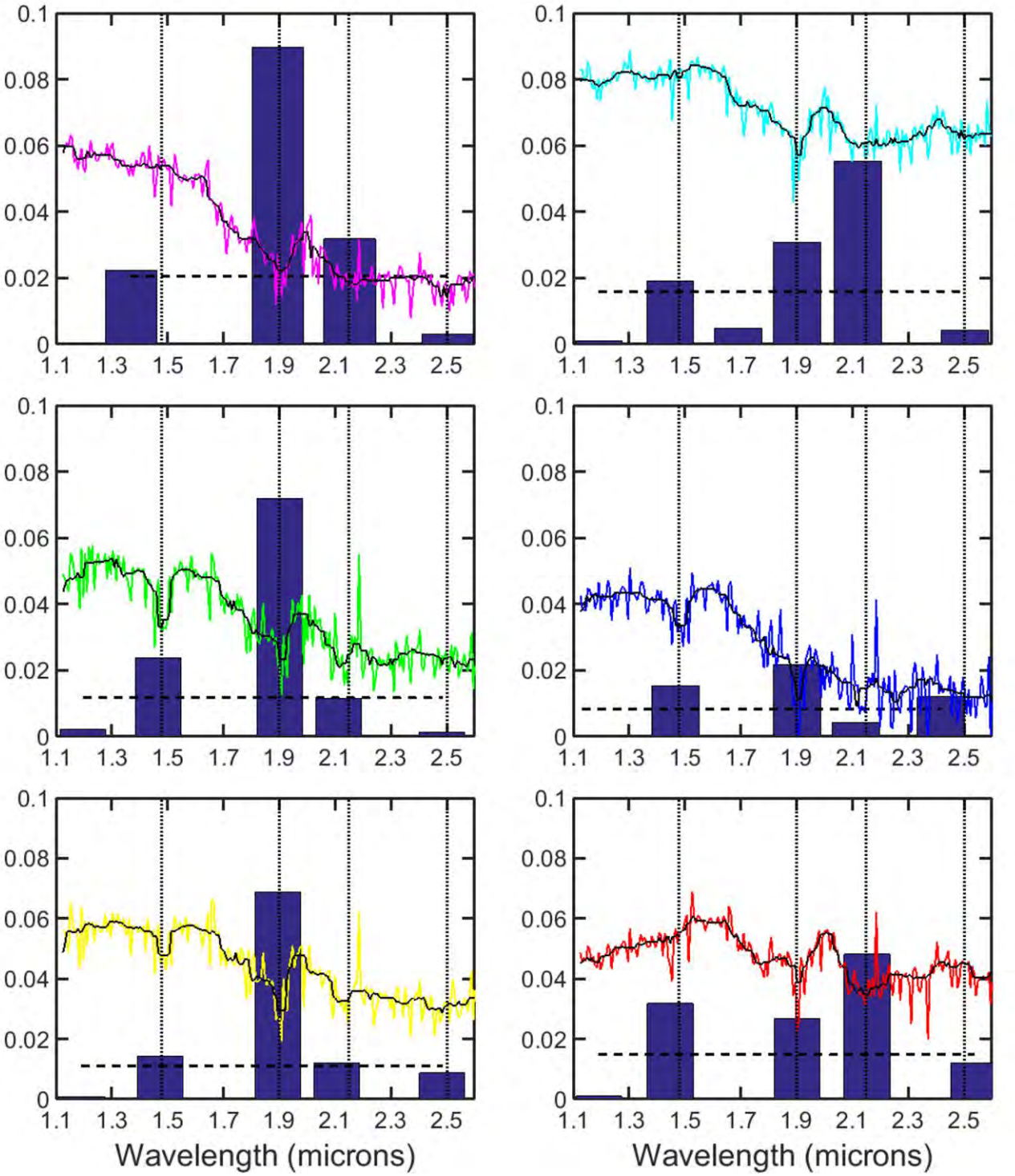

Fig S2. Signal verification for Palikir using band-detection algorithm. Each plot corresponds to one of the six pixels from Fig. 1 where a hydration band is observed. The bars show areas of the detected

bands at wavelengths of hydration combinations and overtones, where the y-axis shows area of the absorption band. The horizontal dashed lines show the mean of areas of all detected "bands" at any wavelength, which is taken to represent the noise threshold for band detection. The 4 vertical dotted lines mark the same wavelengths as Fig. 1.

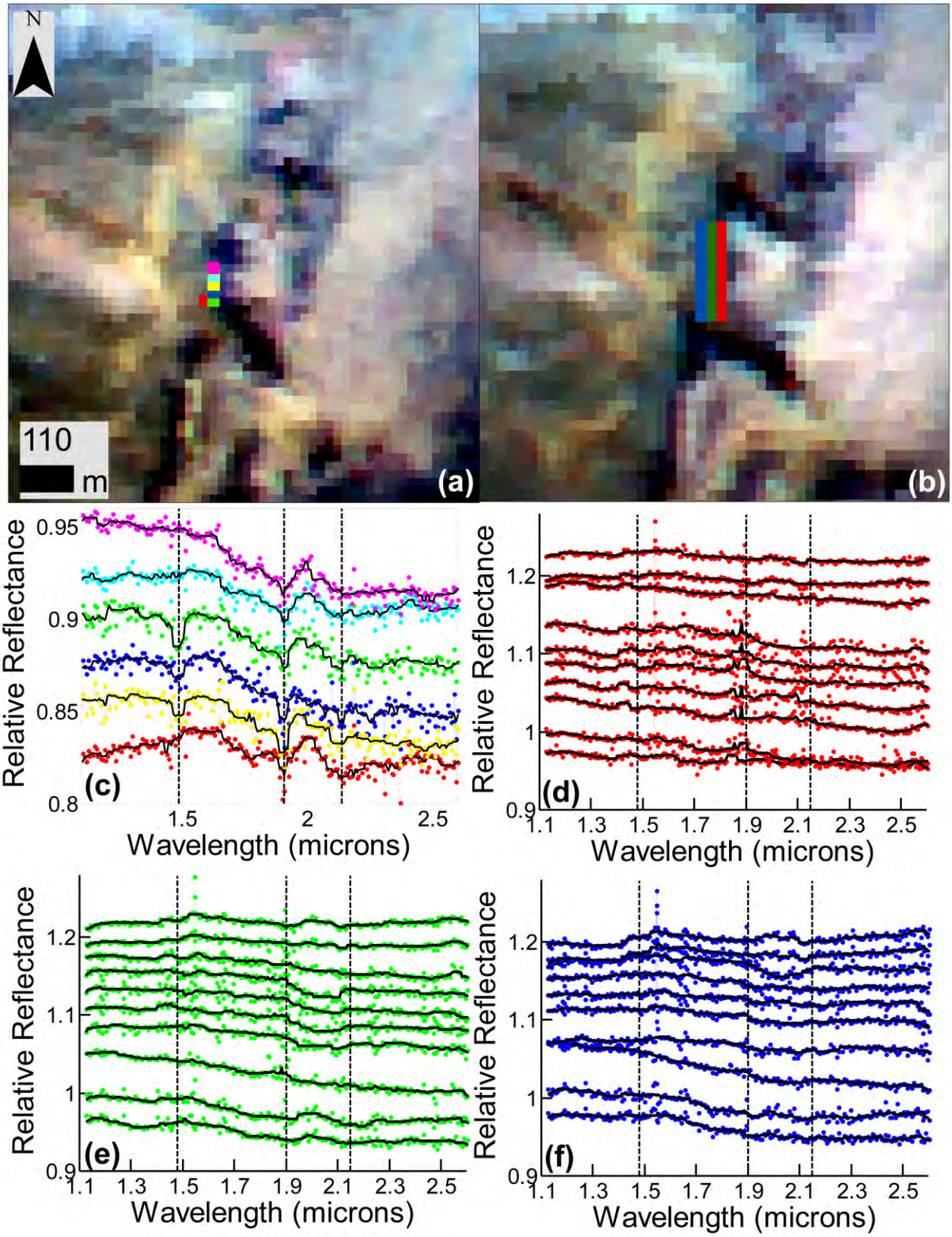
N
110
m
(a)
(b)
Relative Reflectance
0.95
0.9
0.85
0.8
(c)
1.5
2
2.5
Wavelength (microns)
Relative Reflectance
1.2
1.1
1
0.9
(d)
1.1 1.3 1.5 1.7 1.9 2.1 2.3 2.5
Wavelength (microns)
Relative Reflectance
1.2
1.1
1
0.9
(e)
1.1 1.3 1.5 1.7 1.9 2.1 2.3 2.5
Wavelength (microns)
Relative Reflectance
1.2
1.1
1
0.9
(f)
1.1 1.3 1.5 1.7 1.9 2.1 2.3 2.5
Wavelength (microns)

Fig S3. CRISM data of Palikir crater RSL from the same region but at two different times. **(a)** CRISM observation FRT0002038F of Palikir crater, and the six pixels where the hydration band is observed. **(b)** CRISM observation FRT0001E24D with regions of interest (red, green and blue pixels) shown, which was used to generate spectra. Scale and N-arrow for both (a) and (b) are the same. Both images use the same CRISM bands for the RGB as Fig. 1b **(c)** Spectra from all the pixels shown in (a). **(d)** Normalized spectra from all the red pixels in (b). **(e)** Same as (d) but for the green pixels. **(f)** Same as (d) for the blue pixels. All are shown ratioed to nearby non-RSL material.

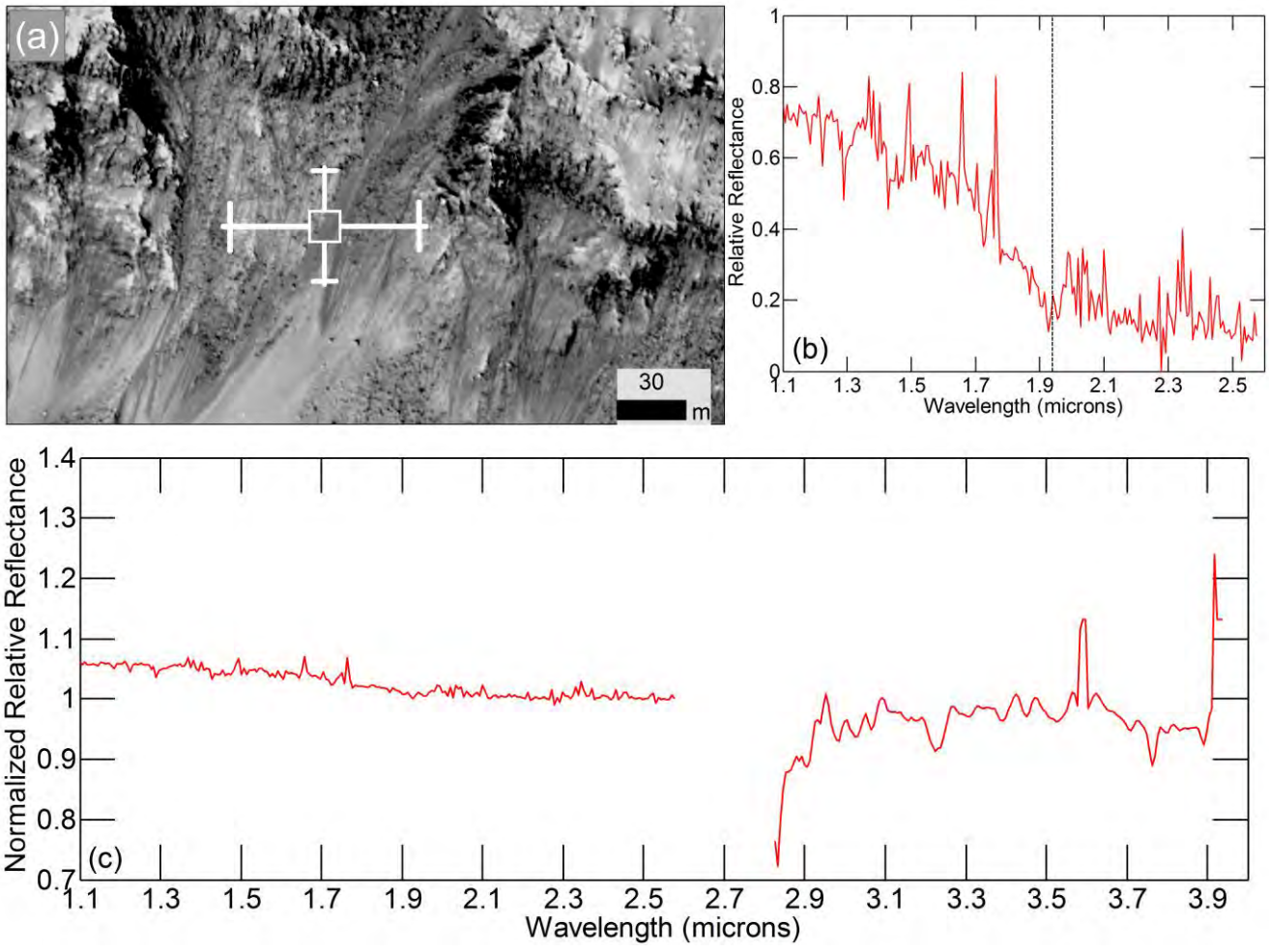

Fig S4. RSL in Palikir crater from MY 31 and its spectrum. **(a)** ESP_032381_1380 (Ls: 340, MY: 31): Orthorectified HiRISE observation of the same area as Fig. 1 (a), but from a different Mars year showing the recurring aspect of RSL. White box with error bars showing the approximate location of the CRISM pixel analyzed. **(b)** CRISM spectrum of the regions seen in (a), ratioed to nearby non-RSL material. The red spectrum is from MY 31 of approximately the same spot (coordinated CRISM observation FRT00029F0C). (c) Same as (b), but the spectrum extends from 1.1 μm to 4.0 μm and is normalized to relative reflectance at 2.6 μm. A broad absorption at ~3 μm is clearly seen.

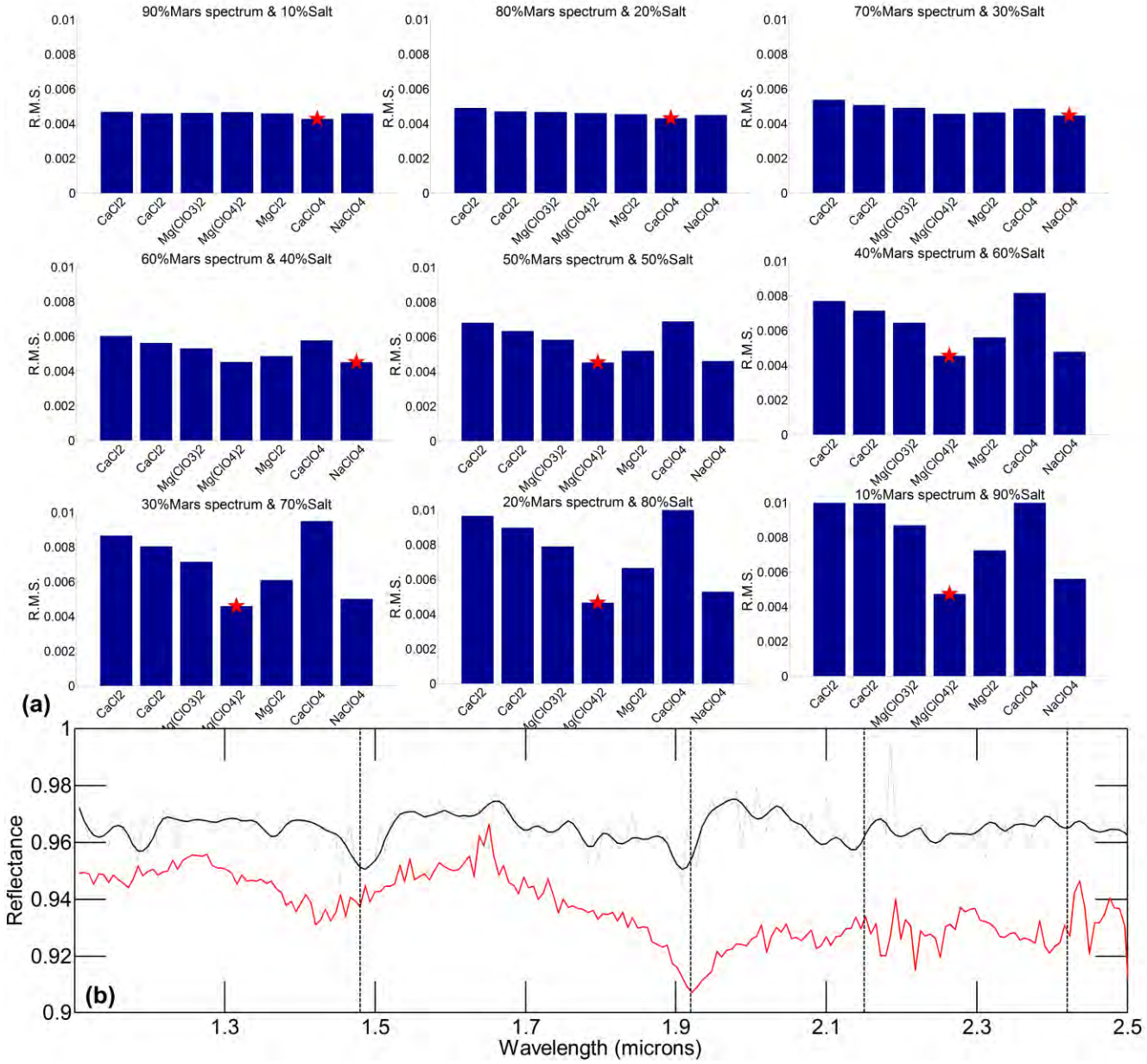

Fig S5. Misfit between Palikir RSL and laboratory spectra. **(a)** The nine plots here show the misfit between the observed spectrum and laboratory spectra of single salt species as a function of their proportions. The title of each slide reports the proportion of each spectrum used in the model. The Y-axis is the total root-mean square error between the two spectra. The X-axis corresponds to single salts used in the model. The bar with red star denotes the linear combination of the salt and Mars spectrum that results in the lowest misfit (i.e. best match). **(b)** Result from least-square regression analysis. The

black spectrum is from Palikir crater, and the red laboratory spectrum is the best matched, which is a linear combination of the Martian soil (62%) and multiple salts (magnesium perchlorate (23.15%), chlorate (12.5%), and chloride (1.5%)). Perchlorates can explain the narrowness of the observed absorptions, but the inability to match the exact wavelength of the 1.48-μm band suggests the presence of an additional salt.

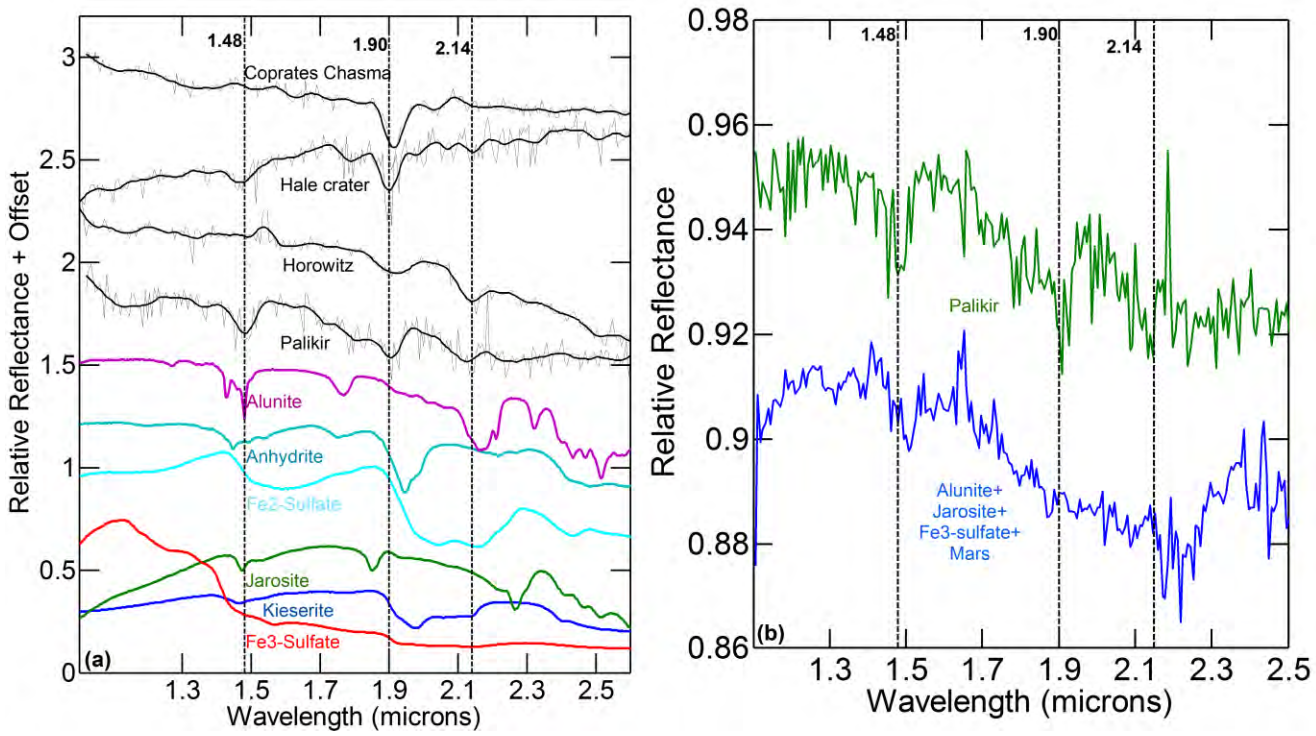

Fig S6. Spectra of various sulfates and RSL sites and result from linear spectral mixture. **(a)** Infrared laboratory spectra of various sulfates in color, and of the four RSL sites in solid black color lines. **(b)** The blue spectrum is the result from spectral mixing between alunite (11.56%), jarosite (26.78%), Fe3-sulfate (19%) and Martian soil (42.65%). The green spectrum is of Palikir crater for comparison.

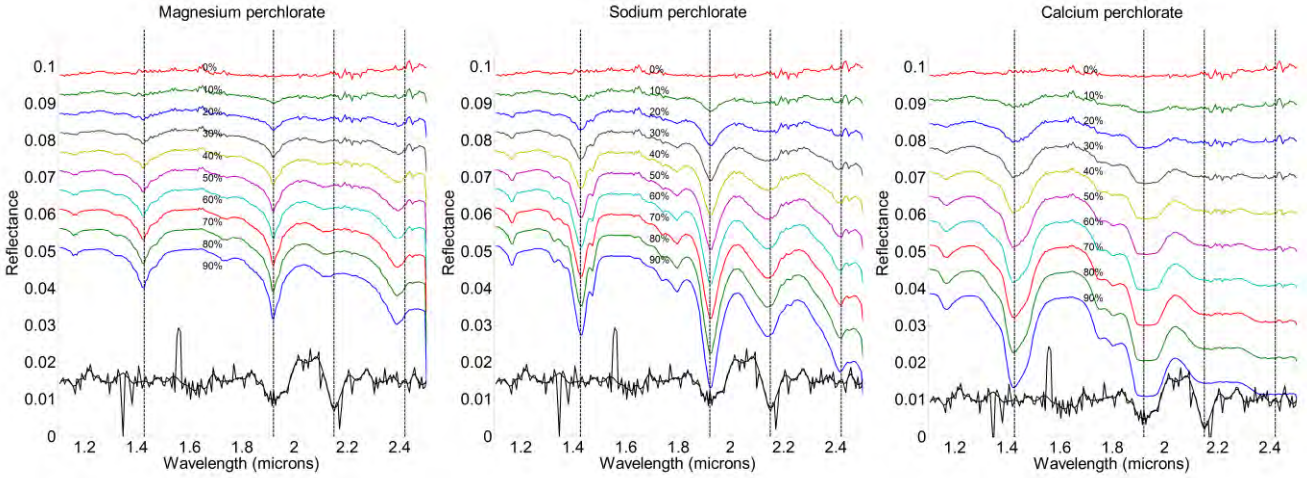

Fig S7. Linear spectral mixture result for Horowitz crater. The three plots show the Horowitz spectrum in black and results from linear spectral mixtures between Martian soil and various salts (specified in the title) as a function of the proportion. The text in black near each curve shows the proportion of the salt spectrum used in that model. A linear combination of sodium perchlorate and Martian soil is the only mixture that is able to recreate the shape of the 2.15 μm feature observed in the Horowitz RSL slope spectrum, but it predicts a stronger 1.4-μm absorption than is observed. Alternatively a non-perchlorate salt may be responsible for the 2.15-μm band.

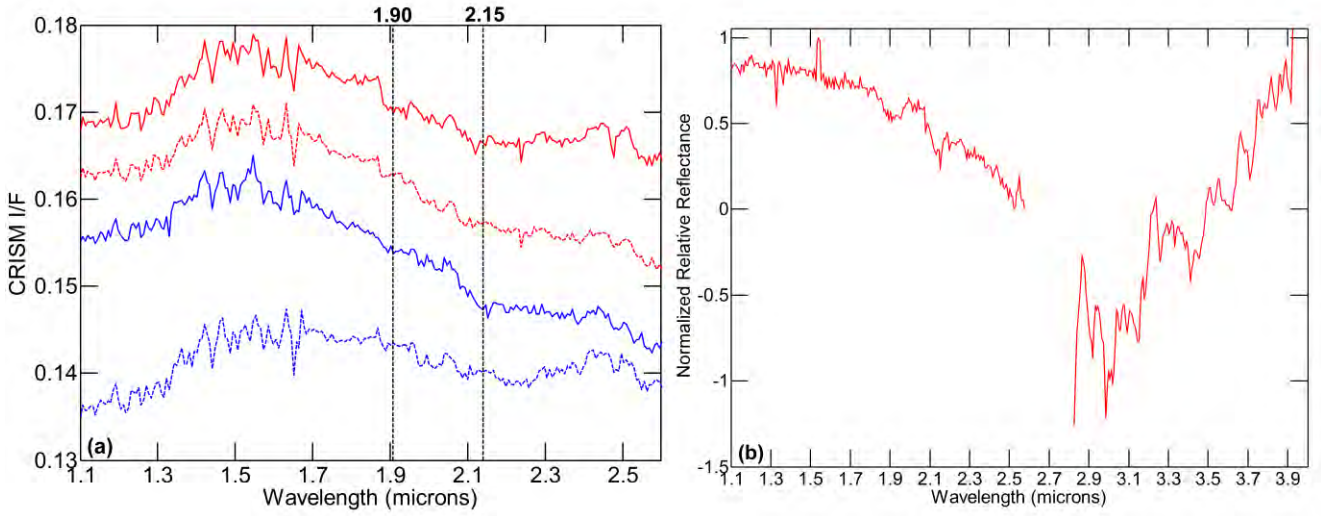

Fig S8. Spectrum of RSL slopes from Horowitz crater. (a) Spectra from FRT00008573 of RSL region in solid color lines and corresponding denominator areas in dashed color lines. (b) CRISM reflectance spectrum of the RSL pixels from FRT00008573, ratioed to nearby non-RSL material and normalized to relative reflectance at 2.6 μm, showing a deep absorption band at ~3 μm.

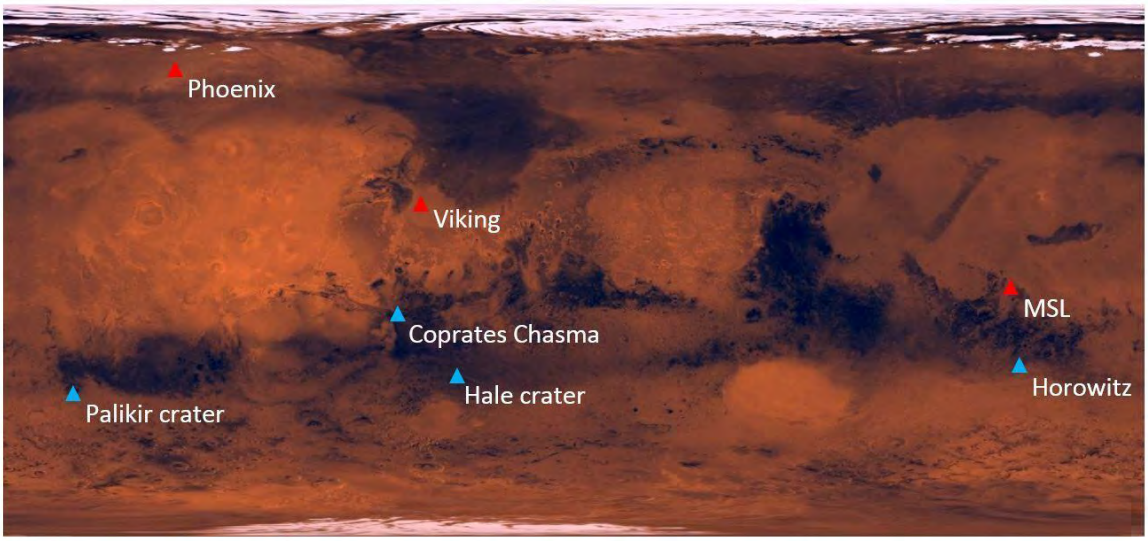

Fig S9. Distribution of sites where perchlorate has been detected. In red: in-situ detection of perchlorates via surface missions. In blue: Sites discussed in this paper. Background is colorized global Viking mosaic .

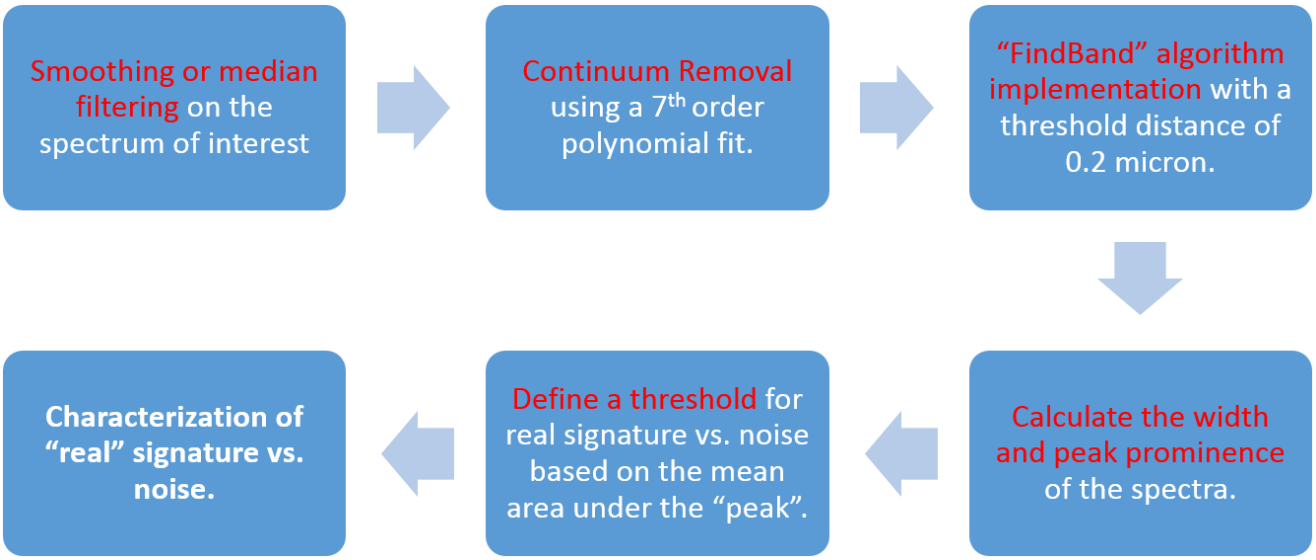

Fig S10. Flow chart for the band detection algorithm routine used in this study to elucidate signal from noise.

Table S1.

HiRISE_ID	**CRISM_ID**	**L_s^o**	**Approximate co-ordinates of RSL in CRISM (Samples/Lines)**
Palikir Crater (-41.6°N, 202.3°E)			
G11_022478_1382_XN_41S157W*	FRT0000E24D	292	N/A
ESP_024034_1380	FRT0002038F	359	335/218, 335/226, 335/232, 336/218, 336/242, 336/247
ESP_030891_1380	FRT00028CEB	273	N/A
ESP_031102_1380	FRT00028FE2	283	N/A
ESP_032381_1380	FRS00029F0C	340	312, 58
Horowitz Crater (-32.0°N, 140.8°E)			
PSP_005787_1475 (Fig 2.a)	FRT00008573	334	379,233
PSP_005787_1475 (Fig 2.b)	FRT00008573	334	339,73
Coprates Chasma (-14.7°N, 304.6°E)			
ESP_031019_1650	FRS00028E0A	279	Multiple location with 1.9 absorption in the fan. See Fig. 4.
Hale Crater (-35.7°N, 323.5°E)			
ESP_032416_1440	FRS00029F84	342	335,96-98

Table. S2

HiRISE_ID	**CRISM_ID**	**L_s^o**	**Approximate co-ordinates of denominator and non-RSL region (in italics) in CRISM un-projected (Samples/Lines)**
Palikir Crater (-41.6°N, 202.3°E)			
ESP_024034_1380	FRT0002038F	359	*317/221, 316/216, 316/210, 315/209, 345/291, 345/285 345/278, 345/276* 336/30-54 335/30-54
ESP_032381_1380	FRS00029F0C	340	312, 5-20
Horowitz Crater (-32.0°N, 140.8°E)			
PSP_005787_1475 (Fig. 2a)	FRT00008573	334	379/352-358
PSP_005787_1475 (Fig. 2b)	FRT00008573	334	339/37-43
Coprates Chasma (-14.7°N, 304.6°E)			
ESP_031019_1650	FRS00028E0A	279	Multiple location with 1.9 absorption in the fan. Multiple denominators used.
Hale Crater (-35.7°N, 323.5°E)			
ESP_032416_1440	FRS00029F84	342	335/54-60